J Comput Aided Mol Des (2010) 24:237–256
DOI 10.1007/s10822-010-9336-6

Using a homology model of cytochrome P450 2D6 to predict substrate site of metabolism

Rayomand J. Unwalla · Jason B. Cross · Sumeet Salaniwal · Adam D. Shilling · Louis Leung · John Kao · Christine Humblet

Received: 29 September 2009 / Accepted: 15 March 2010 / Published online: 2 April 2010

Abstract CYP2D6 is an important enzyme that is involved in first pass metabolism and is responsible for metabolizing ~25% of currently marketed drugs. A homology model of CYP2D6 was built using X-ray structures of ligand-bound CYP2C5 complexes as templates. This homology model was used in docking studies to rationalize and predict the site of metabolism of known CYP2D6 substrates. While the homology model was generally found to be in good agreement with the recently solved apo (ligand-free) X-ray structure of CYP2D6, significant differences between the structures were observed in the B′ and F–G helical region. These structural differences are similar to those observed between ligand-free and ligand-bound structures of other CYPs and suggest that these conformational changes result from induced-fit adaptations upon ligand binding. By docking to the homology model using Glide, it was possible to identify the correct site of metabolism for a set of 16 CYP2D6 substrates 85% of the time when the 5 top scoring poses were examined. On the other hand, docking to the apo CYP2D6 X-ray structure led to a loss in accuracy in predicting the sites of metabolism for many of the CYP2D6 substrates considered in this study. These results demonstrate the importance of describing substrate-induced conformational changes that occur upon binding. The best results were obtained using Glide SP with van der Waals scaling set to 0.8 for both the receptor and ligand atoms. A discussion of putative binding modes that explain the distribution of metabolic sites for substrates, as well as a relationship between the number of metabolic sites and substrate size, are also presented. In addition, analysis of these binding modes enabled us to rationalize the typical hydroxylation and *O*-demethylation reactions catalyzed by CYP2D6 as well as the less common *N*-dealkylation.

Keywords Cytochrome P450s · CYP2D6 · Homology modeling · Molecular docking

Rayomand J. Unwalla and Jason B. Cross contributed equally to this work.

Electronic supplementary material The online version of this article (doi:10.1007/s10822-010-9336-6) contains supplementary material, which is available to authorized users.

R. J. Unwalla (✉) · J. B. Cross · S. Salaniwal
Chemical Sciences, Wyeth Research, S-2421, 500 Arcola Road, Collegeville, PA 19426, USA
e-mail: unwallr@wyeth.com

Present Address:
R. J. Unwalla
Pfizer Research, 445 Eastern Point Road, Groton, CT 06340, USA

A. D. Shilling · L. Leung · J. Kao
Drug Safety and Metabolism, Wyeth Research, 500 Arcola Road, Collegeville, PA 19426, USA

C. Humblet
Chemical Sciences, Wyeth Research, 865 Ridge Road, Princeton, NJ 08543, USA

Present Address:
J. B. Cross
Cubist Pharmaceuticals, Inc., 65 Hayden Avenue, Lexington, MA 02421, USA

Present Address:
S. Salaniwal
Accelrys, Inc., 10188 Telesis Court, San Diego, CA 92129, USA

Introduction

Drug discovery has become an increasingly complex, time consuming and expensive process. As a result, there is an

increased focus on developing drugs with enhanced therapeutic performance in terms of efficacy, safety and improved patient compliance [1]. A significant number of adverse drug reactions can be attributed to drug–drug interactions where administration of one drug can result in the inhibition of metabolism of other co-administered drugs. Thus, early consideration of drug metabolism has become more important in early stages of drug development.

Cytochrome P450s are a large family of heme containing enzymes that are responsible for the oxidative metabolism of a wide variety of drugs, environmental chemicals, and endogenous compounds [2]. The underlying mechanism of this reaction involves binding of molecular oxygen to the heme group to give rise to activated iron-oxygen species, which can react with substrates through a variety of mechanisms including epoxidation, *N*-dealkylation, *O*-dealkylation, *S*-oxidation and hydroxylation [3] (Fig. 1). Amongst the several isozymes of CYP450, CYP2D6 is an important isozyme involved in oxidative metabolism of several drugs [4]. Although the expression level of CYP2D6 is only 2% of all the hepatic CYPs, it is implicated in the metabolism of ~25% of currently marketed drugs. Many antidepressants and antipsychotic medications are metabolized by this enzyme [5]. These compounds represent a variety of chemical structures, however, they all share a common feature, namely the presence of a basic nitrogen at a distance of approximately 5, 7 or 10 Å from the site of oxidation and planar aromatic rings [6]. In addition, due to the polymorphic expression of CYP2D6 in humans, drug–drug interactions via inhibition of this CYP enzyme are particularly undesirable [7]. For example, 5–10% of European and North American Caucasians who are deficient in this enzyme due to genetic mutation have defective metabolism for drugs that are CYP2D6 substrates. The inability of these subjects to turn over these compounds leads to accumulation of toxic levels of the drug in the body, resulting in serious life threatening conditions [8]. Thus, characterization of potential sites of metabolism (SoM) within the substrates is important when designing new compounds with improved pharmacokinetic profiles and in avoiding the presence of toxic metabolites. However, the experimental elucidation of the site of metabolism is usually a highly resource-demanding task, requiring several experimental techniques and consuming a considerable amount of compound. In silico prediction methods such as MetaSite [9], which rely on the fingerprint similarity between the computed 3D structure and GRID-based representation of the CYP enzymes, are able to predict the principal SoM in 78% of the cases when using the top three predictions. However, this accuracy drops to 55% when only the top ranked prediction is considered [10]. Several other computational approaches, such as pharmacophore models [11] for 2D6 substrates, have been published, but it has become clear that no single model can account for the diversity of all substrates. For example, while it's true that the majority of CYP2D6 substrates do contain a basic nitrogen, there are some exceptions, such as progesterone [12] and spirosulfonamide [13].

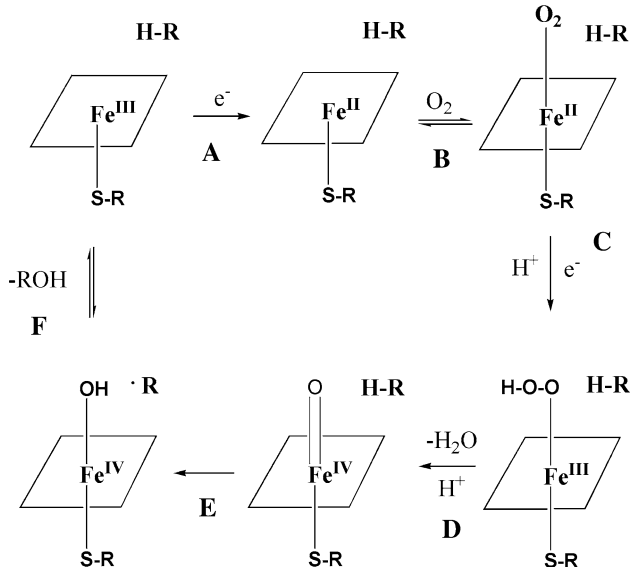

Fig. 1 Cytochrome P450 catalytic cycle for a hydroxylation reaction. S represents the sulfur atom of Cys, which is coordinated with the heme iron in the active site. This is a multi-step mechanism; (*a*) substrate (R–H) binding and transfer of first electron, (*b*) binding of molecular oxygen, (*c*) transfer of second electron followed by (*d*) proton transfer and cleavage of O–O bond, (*e*) abstraction of hydrogen atom from the substrate, and (*f*) product release

In recent years the availability of structural information for many mammalian cytochrome P450s, for example CYP2A6 [14], CYP3A4 [15, 16], CYP2C5 [17, 18] and CYP2C9 [19, 20] has provided a wealth of information on how various substrates and inhibitors interact within the binding cavity. While these structures do provide useful information, they still pose challenges in interpreting biological data, as seen in the case of the crystal structure of CYP2C9 bound with warfarin. Here the ligand was found to bind in a non-productive orientation in a distal cavity with the known 6 and 7 hydroxylation sites located approximately 10 Å away from the iron in the heme cavity. A subsequent CYP2C9 structure with the substrate flurbiprofen bound revealed correctly the ligand's primary site of oxidation (i.e., 4′ position) was located ~5 Å from the iron heme pocket [20]. In addition, several CYPs have only been crystallized in the apo form and for some of these structures it is not clear whether the crystal structure corresponds to an active state [21]. Finally, a comparison between the ligand-bound and ligand-free crystal structures of many CYPs shows a ligand induced binding pocket that is able to accommodate ligands of diverse size and structure.

There are no published substrate-bound X-ray structures of CYP2D6, however an apo form of the CYP2D6 structure became available [22] while our studies were in progress. The structure has been able to shed light on the role of important amino acid residues, such as Glu-216 and Asp-301, in substrate recognition. Both these residues have been proposed to play a role in the binding of substrates and inhibitors, with Glu216 likely acting as a recognition residue that interacts with basic ligands and forms an intermediate binding site prior to substrate migrating to a reactive position within the cavity and interacting with Asp-301. Manual docking studies on substrate debrisoquine do indeed show that this ligand can fit into an "intermediate pocket" formed between Glu-216 and Phe-483, as well as dock into the reaction site with the substrate bound between Phe-120 and Phe-483 residues. It was proposed that in this position the guanidine group of the substrate could form a salt bridge with Asp-301 if an alternative rotameric state to that found in the crystal structure was invoked.

Automated molecular docking has become an important computational tool for predicting protein–ligand interactions, however, the accuracies of docking methods differ widely with the docking algorithms and scoring functions used. A recent study [23] assessed the ability of docking-based virtual screening methods to predict the SoM of 65 known CYP2D6 substrates by using multiple docking programs and scoring functions. The consideration of water molecules at predicted positions within the active site during docking and rescoring of pooled docked poses from four different docking programs (Autodock, ChemScore, FlexX, GOLD-Goldscore and Gold-Chemscore) with the SCORE scoring function improved the success of correctly identifying the experimentally observed site of metabolism for 80% of the ligands. While 80% success is optimal, the use of multiple docking methods and scoring functions is more problematic, since it is a time consuming and potentially an impractical strategy to predict binding mode of substrates. Here we present an extensive docking study to predict the SoM of 16 known CYP2D6 substrates using a single docking program, Glide [24].

With a goal of developing a computational model that provides predictive capability regarding the inhibition and substrate activity of this enzyme, we have built a homology model of CYP2D6 based on published X-ray structures of human CYP2C5 complexes. The homology model was then refined, validated, and used in docking studies with Glide. There are several main objectives of this study. First, we aimed to develop a docking strategy that is fast, easy to use and computationally inexpensive for predicting SoM of various known CYP2D6 substrates and secondly investigate if a three dimensional method can provide valuable insight into its function. Lastly, we compared the homology model with the recently solved substrate-free CYP2D6 X-ray structure and identified key differences between these structures.

Methods

Homology modeling of CYP2D6

CYP2D6 is one of the most widely studied [25] P450 isoform due to its importance in the metabolism of CNS drugs. Several homology models have already been described [26, 27] with varying accuracy in the substrate region and in predicting stereoselective metabolism. The interested reader is referred to a comprehensive study by de Graff et al. [28] on homology model guided site directed mutagenesis studies of CYP2D6.

The primary amino acid sequence used for building the homology model is identical to the CYP2D6 X-ray sequence [22] except for two mutations distant from the active site, L230D and L231R, which were done in order to improve the solubility and expression levels of the X-ray crystal construct. The homology model of human CYP2D6 was constructed based on the available crystal structures of rabbit CYP2C5 substrate-bound structures [17, 18] (PDB codes 1NR6 and 1N6B) using the comparative modeling program Modeller 6v1 [29], as implemented within the Insight II (Version 2000) module. In general, the homology model building approach was similar to the one described earlier [28]. The CYP2C5 structure was chosen because of its higher sequence similarity (full length) with CYP2D6 (58%) compared to other CYP structures that are currently available. The primary sequence identity between CYP2C5 and CYP2D6 is 41%. This high degree of similarity indicates that it should be possible to build a model of good quality. Primary amino acid sequence alignment was done first using the Align_2D feature within Modeller, as shown in Fig. 2, and then 50 models were generated using the restraint-based method. Subsequently, five models with lowest values for the modeler objective function, also referred to as the probability density function (pdf), were evaluated further using the DOPE (Discrete Optimized Protein Energy) scoring function [30], as implemented in the stand alone version of Modeller 9v4.

Model evaluation

The DOPE scoring function, which is a distance-dependent statistical potential derived from a non-redundant PDB subset of high resolution structures, was used for model assessment. This will be discussed briefly in the next section. The model with the lowest DOPE score was subjected to Ramachandran analysis using MOLPROBITY [31],

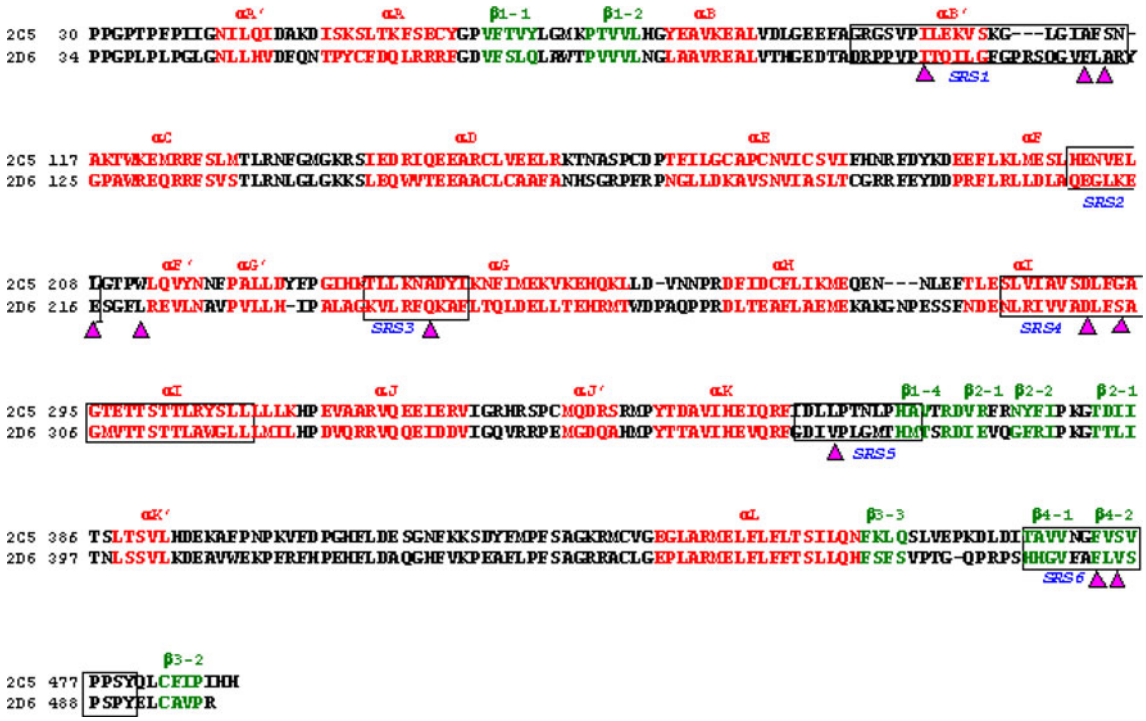

Fig. 2 Alignment of the CYP2D6 and CYP2C5 sequences with secondary structure indicated. Secondary structure elements, i.e., helices are shown in *red* and strands as *green* in the alignment. Residues that belong to the six Structure Recognition Sites (SRSs) as defined in Ref. [28] are enclosed in *boxes* and key residues that contribute to ligand recognition are marked by *triangles*

which evaluates each side chain conformation against an updated rotamer library. The final model possessed good stereochemical quality, since 94% of all residues were located in the favored region and 98% of all residues were found in allowed regions (see Supporting Information).

Finally, the homology model was validated based on its ability to dock the known CYP2D6 substrate codeine in the binding mode determined by NMR spin-relaxation studies [32] using the Glide program. These details are presented in the Supporting Information section.

Protein structure preparation for docking

Starting with the CYP2D6 homology model, several modifications were made, using the Maestro graphical user interface [33], in order to prepare the structure for docking. The heme iron cation was given a "+2" charge. The thiol side chain of Cys-443 remained protonated even though the sulfur is coordinated to the heme iron. This approximation should result in minor systematic errors that have little effect on the docking results. In the current version of Maestro it was not possible to correctly build the iron coordinated heme complex as illustrated in Fig. 1, so some modifications had to be made. In order to approximate the position of the iron coordinated oxygen, a water molecule was placed adjacent to the heme on the side opposite to Cys-443. It was then subjected to optimization using the OPLS-AA force field [34] in MacroModel [24] while holding the protein fixed. The hydrogen atoms were then stripped from the water molecule, the atom type of the oxygen was changed to "OM" (alkoxide or carboxylate atom type) and it was given a "−1" charge in order to approximate the charge separation of the iron oxide (Fe–O bond length was 1.6 Å). All histidine, glutamine, and asparagine side chains in the receptor site were visually inspected and modified as needed, based on the hydrogen bonding networks in the protein. Using the Protein Preparation Wizard in Maestro, the positions of all hydrogen atoms were optimized using restrained minimization.

Receptor grid generation

The center of the box containing the receptor grids was defined by the centroids of the Phe-120 and Thr-309 residues. The size of the bounding box was set to 12 Å in all dimensions, due to the large size of the CYP2D6 binding site. The scaling factors for the van der Waals radii of non-polar atoms (those with an absolute partial charge less than 0.25) were set to 1.00 and 0.80, resulting in two sets of receptor grids that were used for docking. The use of a scaling factor of less than 1.0 softens the potential so that mild amount of steric clash can be tolerated between the

ligand and receptor. It was thought that the inclusion of some degree of this steric overlap could aid in the correct prediction of binding modes of the substrates.

Substrate preparation

Chemical structures of the substrates were taken from the literature. All structures were built using the Maestro interface, with multiple stereoisomers and protonation states, where applicable, enumerated manually. For saturated and partially saturated ring systems, up to 10 low energy ring conformations were generated for each substrate using the LigPrep utility. All conformations were then subjected to minimization using the MMFFs force field [35].

Docking calculations

Flexible docking of substrates was performed using Glide [24] with no defined constraints. Both the standard precision (SP) algorithm [36, 37], with post-docking minimization of poses, and the extra-precision (XP) algorithm [38] were used. Scaling of van der Waals radii for non-polar atoms (those with an absolute partial charge less than 0.15) was set to 0.80 (default) and 0.70 for each docked substrate. Modification of this scaling factor was another way to allow small amount of steric clash in the binding site by reducing the effects of steric overlap between the protein and ligand. Up to 30 poses were saved and visually inspected for each substrate docked.

Results and discussions

Differences between homology model and apo X-ray structure of CYP2D6

The apo X-ray structure of CYP2D6 resolved at 3.0 Å (PDB code 2F9Q) became available during the course of these studies. The residue numbering scheme discussed in this section refers to the CYP2D6 wild type sequence. As expected, the structure shows the characteristic P450 fold as seen in other members of the family. The structure includes residues 52–497 and a short stretch of the proline rich N-terminal region (residues 34–41). Residues within the 42–51 region (i.e., A′ helix) were not resolved in the structure. Additionally, residues within the F–G loop (residues 229–239) were built as alanines, since the electron density maps were insufficiently clear to unambiguously assign the correct residue side chains. Figure 3 shows the DOPE per-residue score of the CYP2D6 X-ray structure superimposed with our homology model. Since the DOPE scores are not absolute, a direct numerical comparison between the two is not possible, however, one can get a qualitative assessment of the model by comparing the shapes of the two profiles for residues 52–497. The profile closely corresponds in many regions on the two structures and the major differences lie mainly in the F to G helical region (residue 229–239). Since the quality of the electron density maps in the published X-ray structure, especially for the F–G loop, was not well resolved (only a polyalanine trace was built for part of this loop), it is not surprising that the profile in this region is completely different. The X-ray structure has 85% of the residues in the favored region and 96% of residues in allowed regions as determined by MOLPROBITY analysis.

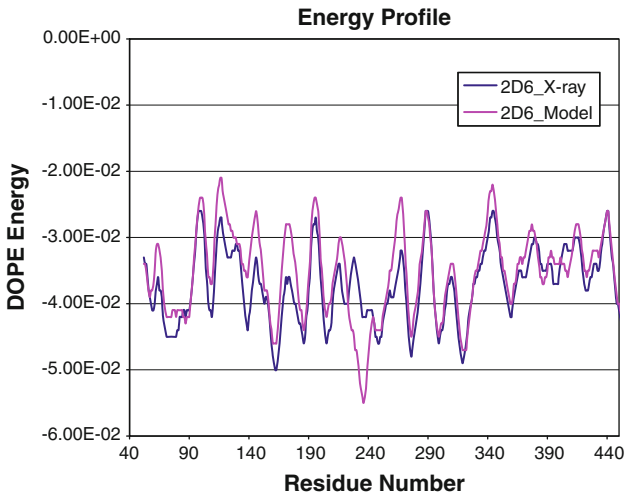

Fig. 3 DOPE per-residue score profiles for the CYP2D6 homology model and apo X-ray structure (PDB 2F9Q, monomer A)

Figure 4 shows an overlay of the CYP2D6 homology model with the X-ray structure, and Fig. 5a and b shows the overall structure of the homology model and active site, respectively. An overall structural alignment of our model with the crystal structure gave a RMSD of 2.9 Å for 426 aligned Cα atoms. Both structures have a well defined active site above the heme group and contain residues that have been implicated in substrate recognition and binding by site directed mutagenesis studies [39, 40]. However, significant differences can be found between the two structures in the helix B′ (residues 106–110) region; in the loop between B′ and C (residues 111–117) and in the position of the F helix and F–G loop (residues 214–240). In the X-ray structure the residues in the B′ helix are shifted slightly away from the heme while the loop between the B′ and C region is shifted towards helix I and is held in position by a hydrogen bond between residue Asn-291 of helix I and the backbone carbonyl group of Arg-115. There is evidence from substrate-bound CYP2C5 X-ray structures that ligand induced changes occurring in the B′ helix region depend on the size and shape of the bound substrate.

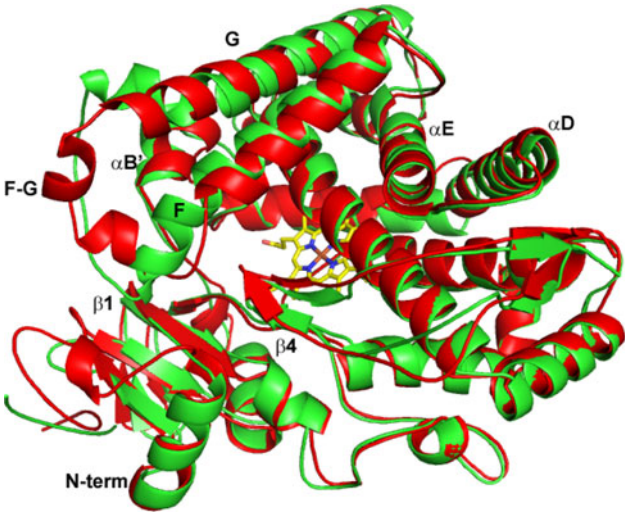

Fig. 4 Overlay of the apo CYP2D6 X-ray crystal structure (PDB 2F9Q, green) with the best homology model (red) of CYP2D6. The heme is depicted in *yellow* and important secondary structure elements are labeled, i.e., α for helices and β for sheets

For example in the CYP2C5/DMZ (1N6B) structure, the B′ helix has shifted roughly ~2.2 Å away from the heme compared to the CYP2C5/diclofenac (1NR6) structure in order to accommodate the larger ligand. It will be interesting to compare this region when a CYP2D6 substrate-bound X-ray structure becomes available. The F helix in the X-ray structure has two additional turns and is shifted slightly away from the β4 sheet region. This change also results in an observed shift in the position of strands 1 and 2 of the β1 sheet between these structures. The F–G loop in the X-ray structure lies across the B′ helix and encloses the side that is open in the model, however, since side chain residues in this region are not well resolved in the X-ray structure, it is difficult to draw any significant conclusions. Other differences, such as in the C–D loop region (residues 141–147), are distant from the active site and not expected to have influence on substrate or inhibitor binding.

We next compared the active sites of our homology model and the crystal structure by examining residues predicted to be involved in the substrate recognition (see Fig. 2) as defined by the six putative Substrate Recognition Sites (SRSs), as described by Gotoh [41]. These sites were proposed based on sequence alignment and mutation studies on CYP2 family proteins and bacterial P450s. All reported point mutations that significantly affect the substrate activity either by direct ligand-CYP interactions or indirectly through changes in the conformation of the

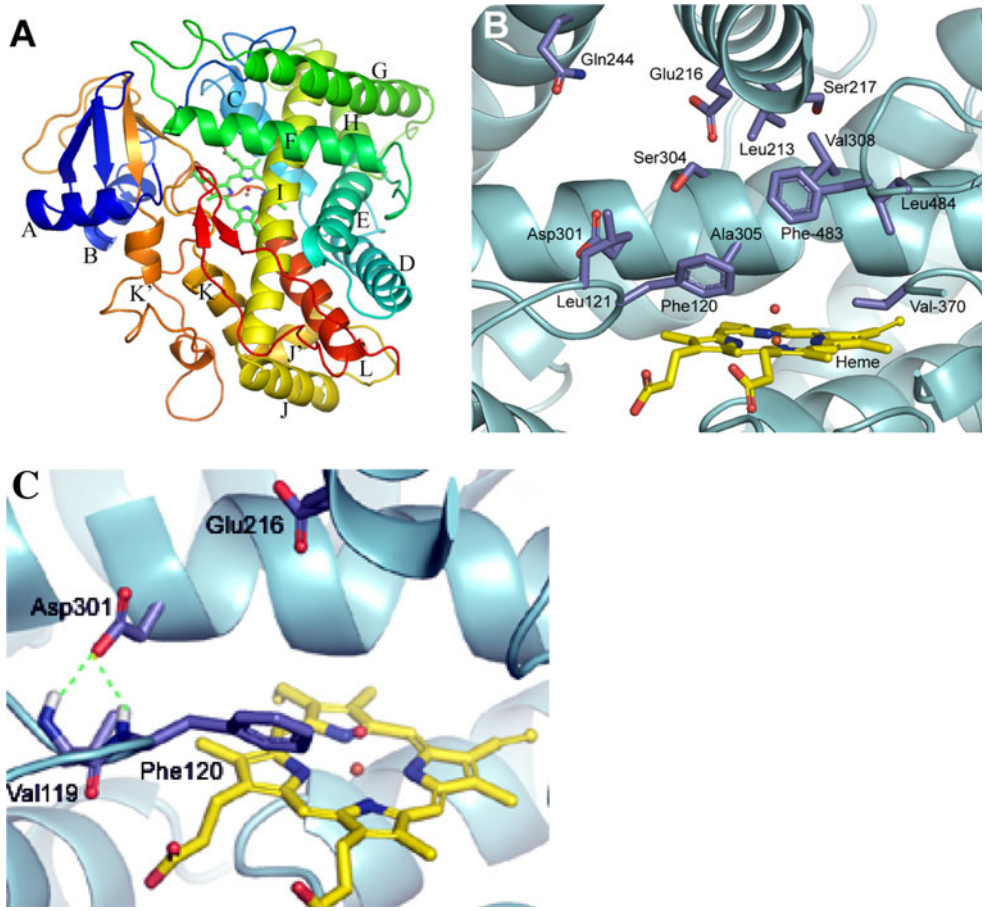

Fig. 5 Structure of the CYP2D6 homology model used for docking calculations. **a** The overall structure of the enzyme with helices labeled. **b** The active site with critical residues labeled. **c** The hydrogen bonds (*colored green*) between the carboxylate group of Asp-301 and the backbone amides of Val-119 and Phe-120 residues of the B′–C loop

active site residues in the CYP2 family proteins fall within these six SRSs. Furthermore, some of the residues in these regions have also been implicated in substrate recognition based on docking studies using known CYP2D6 substrates [23, 28]. The following sections give brief descriptions of the key residues involved in various Substrate Recognition Sites. For some of the key residues within this region, additional discussion is given in the site-directed mutagenesis section.

Substrate Recognition Site 1: This region consists of residues from the B′ helix and the flanking area, i.e., B′-C loop. Important residues believed to be involved in Substrate Recognition Site 1 of CYP2D6 are Val-104, Phe-120 and Leu-121. Of these residues, the major contribution to substrate recognition is from Phe-120, as seen in site directed mutagenesis studies [39]. The role of Phe-120 is to orient the substrate in the active site and define the regiospecificity of the enzyme. Although the location of all three residues in our homology model and crystal structure is similar (Cα(RMSD $\sim$ 0.2 Å)), the Phe-120 residue was slightly displaced towards the heme in the model. The side chain of Phe-120 was in a similar rotameric state as seen in crystal structure, i.e., Chi1 $\sim$ −158, Chi2 $\sim$ 76 degrees.

Substrate Recognition Site 2: The Glu-216 residue from the F-helix is shown to be a major contributor to this substrate recognition site, as seen from various site directed mutagenesis studies [13, 42]. In the description of the crystal structure it was proposed [22] that this residue, along with Phe-483, forms an intermediate substrate binding pocket at the entrance of the solvent channel that may be occupied prior to the substrate migrating to a more "productive" orientation within the cavity. Glu-216 is shifted slightly in the model as a result of the different positioning of the F-helix and reflects a substrate induced conformational change, but the side chain is oriented in a similar way towards the cavity in a trans conformation, i.e., Chi1 $\sim$ 55, Chi2 $\sim$ 177, Chi3 $\sim$ 100 degrees. Further resolution of this residue must await the co-crystallization of substrates with this enzyme.

Substrate Recognition Site 3: This region consists of residues from the N-terminal end of helix G (residues 239–247). In both structures, Substrate Recognition Site 3 is distant from the heme active site and not in position to play a role in substrate binding. However, we don't rule out an indirect effect on ligand binding from residues in this region which can influence the protein conformation. So far no mutation studies have been reported for this region, which makes it difficult to draw any conclusion on its relative importance.

Substrate Recognition Site 4: This region encompasses the Asp-301, Ser-304, Ala-305 and Val-308 residues from helix I. The location and orientation of these residues in the two structures is highly similar. In the crystal structure as well as in the homology model the hydroxyl group of Ser-304 was in a conformation that favors the formation of a hydrogen bond with the backbone carbonyl of Ala-300, thus only leaving the hydrogen bond acceptor site available for substrate binding. However, mutation S304A [43] was found to have no effect on substrate turnover of metoprolol and debrisoquine. These results led the authors to conclude that Ser-304 was not a key ligand-binding residue in the active site of CYP2D6.

Substrate Recognition Site 5: The important residues making up this site, namely Val-370 and Val-374, are located on the loop between helix K and the β1-4 sheet. In both structures the location of these residues is similar. In the crystal structure and the homology model there is a methionine at position 374 instead of valine, which is believed to be present in the wild-type protein. However, experimental data [44] indicate that this amino acid difference does not influence the substrate binding affinities of a range of CYP2D6 ligands as determined from their apparent binding coefficients. Furthermore, the level and stability of expression of CYP2D6 was not influenced by this residue difference, although this mutation did have an influence on the regioselective oxidation (ratio of *O*-demethylation to α-hydroxylation) of metoprolol metabolism.

Substrate Recognition Site 6: This region lies in the loop between the two β strands of sheet 4 and consists of residues Phe-481, Phe-483 and Leu-484. The high temperature factors seen in the X-ray structure for this region suggest some degree of flexibility that could be induced by ligand binding. Mutation studies by Hayhurst and coworkers [45] have shown that both Phe-481 and Phe-483 have similar detrimental effects on the oxidation of debrisquine, however, in both homology model as well as the crystal structure Phe-481 is oriented further away from the active site and not expected to influence substrate binding. The position of Phe-481 makes it difficult to explain the observed mutational results of this residue, however, as suggested by Rowland et al. [22] from constrained molecular dynamics simulation, this loop can alter its conformation and orient both phenylalanines into the cavity. Residues Phe-483 and Leu-484 in both structures are pointed towards the heme group, although the Phe-483 residue in the model is in a different rotameric state, (i.e., Chi1 $\sim$ −93, Chi2 $\sim$ −78 degrees) as a result of the shift in the F-helix. It has been proposed that while both residues can be involved in substrate recognition in this orientation, only Phe-483 can be involved in the reaction site binding.

Site-directed mutagenesis studies of key residues in CYP2D6

Phe-120, Glu-216, Asp-301 and Phe-483 have been implicated as key residues for substrate binding on the basis of previous modeling studies and site directed mutagenesis studies. The two negatively charged residues, Asp-301 and Glu-216, which are separated at a distance of roughly ~13 Å (Cα–Cα distance in the model) in the CYP2D6 cavity, have been implicated in the binding of basic substrates. Asp-301, which is located in the I helix at the base of the active site and adjacent to the Phe-120 residue, was one of the first CYP2D6 residues subjected to site directed mutagenesis studies [13, 40]. Mutation of this residue to a conservative functional moiety, i.e., Glu [46] was shown to have similar catalytic properties to the wild type enzyme towards basic nitrogen containing substrates, i.e., debrisoquine and metoprolol, although some differences in the regioselective oxidation and ligand binding of these substrates were observed. In contrast, substitution of Asp-301 with neutral residues exhibited marked reductions in catalytic activity against the classical CYP2D6 substrates that have basic nitrogen. This data is consistent with the proposal that Asp-301 forms an ion pair interaction with the basic nitrogen of CYP2D6 ligands and thereby facilitates the binding and the orientation of these substrates in the active site. However, in both our homology model and the crystal structure of ligand free 2D6, one of the carboxylate oxygens of Asp-301 forms two hydrogen bonds between the backbone NH groups of Val-119 and Phe-120 from the B′-C loop (Fig. 5C) and thereby suggests an additional role for this residue. Kirton et al. [47] have speculated that Asp-301 may serve to stabilize the B′-C loop in CYP2D6 and possibly other CYPs that contain an acidic residue at this position. This latter hypothesis is supported by mutagenesis studies that show attenuated or total lack of heme incorporation when Asp-301 is mutated to neutral or basic residues. It is interesting to note that in CYP2C5 structures with non-basic substrates bound (i.e., PDB codes 1N6B and 1NR6), Asp-290, which corresponds to Asp-301 of CYP2D6, is also involved in a similar backbone amide interaction with Ile-112 and Ala-113. Thus in the absence of a basic substrate bound CYP2D6 structure that would clearly delineate the role of Asp-301 in ligand binding, we have kept Asp-301 constrained, i.e., hydrogen bonded to backbone amides, in our docking studies. We should add that that the second carboxylate oxygen of Asp-301 can still be involved in ligand recognition by forming a salt bridge with a basic moiety of the ligand. In fact, such a hydrogen bond interaction was observed between the hydroxyl group of the ligand and the Asp-301 side chain (3.04 Å) in our docking studies with basic nitrogen containing substrate metoprolol (see Supporting Information for more details). A situation where Asp-301 could break both hydrogen bonds altogether and adopt a different rotamer to fully engage both carboxylate oxygens in a salt bridge interaction with the ligand would have to depend on the relative energetic contributions of the newly formed hydrogen bond and the cost for protein reorganization for each substrate. Unfortunately, such contributions are not easy to estimate unless one does protein–ligand binding free energy calculations. Previous reports have also suggested [48] that the negative effect on the catalytic activity of mutating Asp-301 is indirect, i.e., Asp-301 role could be to influence the orientation of Phe-120, the side chain which interacts with the aromatic moiety of the substrates.

Examination of the homology model and the crystal structure shows that Glu-216 is positioned at the top of the proposed substrate binding cavity with its side chain pointing towards the heme, consistent with a role in substrate binding. Substitution of Glu-216 with a residue other than Asp [48] strongly attenuated the binding of quinidine, bufaralol and several other CYP2D6 ligands. Catalytic activity with the substrates bufaralol and 4-methoxyphenethylamine was strongly inhibited by neutral or basic mutations at Glu-216 (>95%). Unlike the Asp-301 mutants, the Gln-216 mutant (E216Q) retained 40% enzyme efficiency with the non-basic substrate spirosulfonamide, suggesting that substitutions at Glu-216 affect binding of amine substrates more than others. Further resolution of the importance of the Glu-216 and Asp-301 residues in substrate binding must await the results of the co-crystalization of substrates in this enzyme.

A number of mutation studies have been carried out on Phe-120 which further delineate the role of this residue in substrate and inhibitor binding. Substitution of Phe-120 [49] to alanine abolished the *O*-demethylating activity of 7-methoxy-4-(aminomethyl)-coumarin (NAMC) and altered the relative rates of *O*- versus *N*-demethylation of dextromethorphan. Strikingly, the same mutation did not affect the metabolism of bufaralol. These results suggest that π–π interactions between the substrate's aromatic ring and Phe-120 could play a role in the ligand's orientation within the heme cavity and influence the selectivity and region-specificity of substrate binding and catalysis.

Recent mutation studies on Phe-483 [28] suggest that the influence of this residue on metabolism is strongly substrate dependent. For example in dextromethorphan, two additional metabolites were detected in addition to *O*- and *N*-demethlyated products, while for substrate NAMC no metabolism was seen in the F483A mutant. Most homology models, including ours, show Phe-483 oriented towards the heme and playing a role in ligand recognition.

In summary, the overall structure of our homology model was found to agree well with the X-ray structure.

The differences in the two structures, i.e., F–G helical region and the helix B′ to C region as well as conformational differences of important residues involved in Substrate Recognition Sites, point to important substrate-induced conformational changes, which can be critical in the rationalization and prediction of catalytic activity. Interestingly, similar conclusions were reached by de Graaf and coworkers regarding their homology model [28], which was constructed to guide their site directed mutagenesis studies.

Substrate docking

A total of 16 known CYP2D6 substrates, shown in Fig. 6, were docked to the CYP2D6 homology model. Substrates were chosen from the literature to represent a variety of chemotypes with several different types of metabolic sites (i.e., *O*-dealkylation, *N*-dealkylation, hydroxylation, demethylenation). Many of the CYP2D6 substrates studied have a chiral center. In these cases, both stereoisomers were docked if it was unclear from the literature whether CYP2D6 has a preference for a specific chirality, or if one stereoisomer was preferred but the other still acted as a weak CYP2D6 substrate. If only one stereoisomer was a known CYP2D6 substrate, only that stereoisomer was docked. This increased the total number of docked substrates, including stereoisomers, to 26.

Table 1 presents the results of the docking calculations using both the Glide SP and Glide XP algorithms, along with a variety of settings for van der Waals scaling of the protein and substrates. Stereoisomers that are disfavored, but still act as weak CYP2D6 substrates, are indicated by an asterisk. Success in predicting the SoM by docking was measured based on distance from the oxeme oxygen coordinated to the heme-Fe atom to the SoM on the substrate; if this distance was less than 4.5 Å it was deemed a success. This cut-off was chosen so that results would be roughly consistent with the 6.0 Å cut-off (heme Fe-atom to SoM distance) used by de Graff et al. [23] for catalytic site predictions. Additionally the chosen cut-off is consistent with the distances of ~5.0 Å seen between the site of metabolism and heme iron from substrate bound X-ray structures [20]. The results of each docking calculation were categorized based on whether the docking program

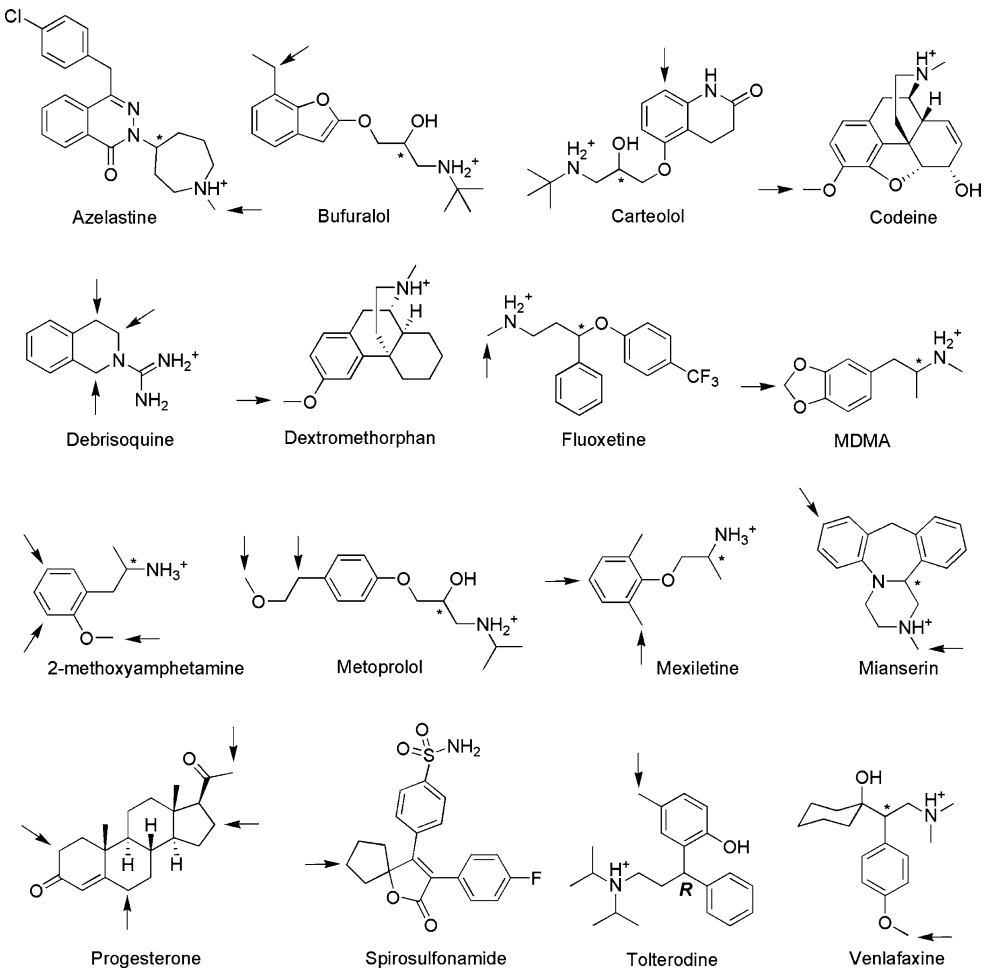

Fig. 6 Chemical structures of CYP2D6 substrates. CYP2D6 sites of metabolism are indicated by *arrows*. Stereocenters are indicated by an *asterisk*

Table 1 Performance of several methods of Glide docking for 26 substrates/stereoisomers

	1.0/0.8[a]		1.0/0.7[a]		0.8/0.8[a]		0.8/0.7[a]	
	SP	XP	SP	XP	SP	XP	SP	XP
(*R*)-Azelastine	–	–	P	–	P	T	P	–
(*S*)-Azelastine	–	–	P	–	P	–	P	P
(*R*)-Bufuralol	P	P	P	P	T	T	P	P
(*S*)-Bufuralol*	P	–	P	–	T	–	T	–
(*R*)-Carteolol	P	P	P	–	P	T	P	P
(*S*)-Carteolol	P	–	P	–	T	T	T	T
Codeine	X	X	–	X	P	–	P	–
Debrisoquine	P	–	P	–	P	–	P	–
Dextromethorphan	T	T	T	T	P	T	P	T
(*R*)-Fluoxetine	P	–	P	–	P	T	P	T
(*S*)-Fluoxetine	–	–	–	–	P	–	–	–
(*R*)-MDMA*	P	T	P	P	T	T	T	T
(*S*)-MDMA	P	–	P	P	T	–	T	P
(*R*)-2-Methoxyamphetamine	P	P	T	P	T	P	P	P
(*S*)-2-Methoxyamphetamine	T	T	T	T	T	P	T	–
(*R*)-Metoprolol	P	–	P	–	P	–	P	–
(*S*)-Metoprolol	T	P	P	–	T	P	T	–
(*R*)-Mexiletine	T	T	P	T	T	T	T	T
(*S*)-Mexiletine	P	T	T	T	T	T	T	T
(*R*)-Mianserin	T	–	T	T	T	T	P	T
(*S*)-Mianserin	–	–	P	–	P	–	P	–
Progesterone	X	X	X	X	T	X	T	T
Spirosulfonamide	X	–	X	–	T	–	P	–
(*R*)-Tolterodine	–	–	–	–	P	T	T	–
(*R*)-Venlafaxine	–	–	P	T	T	–	T	T
(*S*)-Venlafaxine*	P	P	P	–	T	–	P	T
Top pose	5	5	5	6	15	11	11	10
Any pose	17	10	21	10	26	14	25	15

T = Top-pose within 4.5 Å, P = any pose within 4.5 Å, – = no pose within 4.5 Å, X = no docked poses returned

Asterisks indicate minor or disfavored stereoisomers

[a] Indicates van der Waals scaling factor of protein and substrate, respectively

identified a top scoring pose placing the SoM within the cut-off, at least one pose anywhere in the ranked list of docked poses had the SoM within the cut-off, no poses placed the SoM within the cut-off, or no poses successfully generated for the substrate. This categorization scheme was also applied to substrates that had more than one SoM, where placement of any SoM within the distance cut-off constituted a success.

Based on this analysis, the Glide SP algorithm with van der Waals scaling set to 0.8 for the protein and 0.8 for the substrates yielded the best results in this study. Glide SP with these settings was able to generate at least one pose within the cut-off in every case, a 100% success rate. It was also able to identify a top scoring pose within the cut-off in 15 cases (58% success rate). When the analysis was extended to additional poses beyond the top scoring one (Table 2), the results were consistently improved, with an 85% success rate for identifying the SoM if the five top scoring poses were inspected.

Table 2 Success rates for 26 substrates/stereoisomers when examining the top 1, 2, 3, 4, and 5 ranked poses for SoM prediction

No of poses inspected	No of successes	Success rate (%)
1	15	58
2	17	65
3	19	73
4	20	77
5	22	85

This data is for Glide SP with van der Waals scaling of 0.8 for both protein and substrate

The results for Glide XP, even using the same van der Waals scaling mentioned above, were not as impressive. A top-scoring pose was within the cut-off only 42% of the time, while the success rate for identifying any pose within the cut-off was only 54%. In cases like progesterone, where Glide SP was able to find a top-scoring pose within the cut-off, Glide XP failed to return any docking solutions. This may be due to a more stringent treatment of steric clashes in the Glide XP algorithm that cannot be compensated by the softening of the van der Waals radii, although it should be noted that using a scaling factor of 0.7 on the substrate resulted in the generation of a top-scoring pose for progesterone within the cut-off.

Docking was also carried out using the publicly available X-ray structure instead of the homology model. Results for docking the CYP2D6 substrates with the Glide SP algorithm are listed in Table 3. Regardless of the van der Waals scaling used on the protein and substrates, the homology model consistently outperformed the X-ray structure. The lower performance of the X-ray structure points to the fact that there are putative induce-fit effects that cannot be accounted for in the apo structure with a rigid receptor docking program. Since the X-ray structure contains no bound ligand, the protein may not be in a productive conformation for substrate binding. Although a limited amount of steric clash between the ligand and the enzyme is approximated by varying the van der Waals scaling during docking, this is apparently not enough to allow substrates to reliably adopt poses that are consistent with their known SoM. In contrast, the homology model was built from a template containing a bound ligand that may have induced a protein conformation that can be used to successfully identify the SoM of known substrates.

Table 3 Comparison of homology model (HM) and X-ray structure for predicting SoM using Glide SP

	1.0/0.8[a]		1.0/0.7[a]		0.8/0.8[a]		0.8/0.7[a]	
	HM	X-ray	HM	X-ray	HM	X-ray	HM	X-ray
(*R*)-Azelastine	–	X	P	X	P	P	P	T
(*S*)-Azelastine	–	X	P	–	P	T	P	T
(*R*)-Bufuralol	P	P	P	T	T	P	P	P
(*S*)-Bufuralol*	P	T	P	P	T	P	T	P
(*R*)-Carteolol	P	P	P	–	P	–	P	–
(*S*)-Carteolol	P	–	P	–	T	–	T	–
Codeine	X	X	–	X	P	P	P	P
Debrisoquine	P	T	P	P	P	P	P	P
Dextromethorphan	T	X	T	–	P	P	P	–
(*R*)-Fluoxetine	P	T	P	T	P	T	P	P
(*S*)-Fluoxetine	–	T	–	T	P	P	–	T
(*R*)-MDMA*	P	P	P	P	T	P	T	P
(*S*)-MDMA	P	P	P	–	T	P	T	P
(*R*)-2-Methoxyamphetamine	P	T	T	P	T	T	P	P
(*S*)-2-Methoxyamphetamine	T	T	T	T	T	T	T	T
(*R*)-Metoprolol	P	T	P	T	P	P	P	P
(*S*)-Metoprolol	T	T	P	P	T	P	T	P
(*R*)-Mexiletine	T	T	P	T	T	T	T	T
(*S*)-Mexiletine	P	T	T	T	T	P	T	P
(*R*)-Mianserin	T	X	T	T	T	P	P	T
(*S*)-Mianserin	–	P	P	P	P	P	P	T
Progesterone	X	X	X	X	T	T	T	T
Spirosulfonamide	X	–	X	–	T	X	P	T
(*R*)-Tolterodine	–	–	–	–	P	P	T	P
(*R*)-Venlafaxine	–	–	P	–	T	P	T	P
(*S*)-Venlafaxine*	P	–	P	–	T	P	P	P
Top pose	5	10	5	8	15	6	11	9
Any pose	17	15	21	14	26	23	25	23

T = Top-pose within 4.5 Å, P = any pose within 4.5 Å, – = no pose within 4.5 Å, X = no docked poses returned

Asterisks indicate minor or disfavored stereoisomers

[a] Indicates van der Waals scaling factor of protein and substrate, respectively

N-Dealkylation and *O*-demethylation/hydroxylation reactions of CYP2D6 substrates

The well known substrates of CYP2D6 represent a variety of chemical structures, with the common characteristic being the presence of at least one basic nitrogen atom at a distance of 5, 7 or 10 Å from the site of oxidation [6]. Substrates that fit this pharmacophore result in metabolites that favor the usual *O*-demethylation and hydroxylation reactions catalyzed by CYP2D6. On the other hand, the *N*-dealkylation pathway, which is far less common for CYP2D6 catalyzed reactions, results in metabolism at a site adjacent to the basic nitrogen. In this study we included substrates for which experimental evidence is available for the involvement of CYP2D6 in either the *N*-dealkylation or the *O*-demethylation/hydroxylation pathway.

Table 4 gives a detailed description of the docking results for each substrate along with the major metabolic pathway and critical residues involved in substrate recognition. The following discussion relates to identifying features within substrates that favor one pathway over another in our docking studies. For example, why do basic substrates such as azelastine and fluoxetine favor *N*-dealkylation while other basic substrates like bufaralol and dextromethorphan favor the *O*-demethylation/hydroxylation pathway? A detailed description of docked poses for substrates not discussed in this section can be found in the Supporting Information.

Azelastine is an antiallergic and antiasthmatic drug that is metabolized in the human liver via *N*-demethylation to *N*-desmethylazelastine by CYP2D6, CYP3A4, and to a lesser degree by CYP1A2 [50, 51]. Azelastine is a chiral molecule and since it is unclear whether there is a stereospecific preference for oxidation by CYP2D6, both enantiomers were docked to the homology model. For the (*R*)-azelastine stereoisomer, the third highest scoring pose

Table 4 Summary of important structural features of the CYP2D6 substrates

Substrate	Major metabolic transformation	No of sites of metabolism	Chiral preference	Key residues in close contact with ligand[c]	Oxeme-SoM best pose distance[a]	Best ranked pose nearest to oxeme[b]	Major metabolite	No of atoms within 4.5 Å cutoff[d]
(*R*)-Azelastine	*N*-Demethylation	1	Unknown	Phe-120, Asp-301, Leu-484, Ala-305, Leu-121, Ile-106	3.8	3	*N*-Desmethylazelastine	1
(*S*)-Azelastine	*N*-Demethylation	1	Unknown	Ph-120, Leu-484, Leu-121, Ile-106	4.2	8	*N*-Desmethylazelastine	1
(*R*)-Bufaralol	Hydroxylation	1	R	Glu-216[e], Phe-120, Phe-483, Asp-301, Ser-304[e]	3.9	1	1′-Hydroxy bufaralol[g]	1
(*S*)-Bufaralol[h]	Hydroxylation	1	R	Glu-216[e], Ser-304[e]	4.5	1	1′-Hydroxy bufaralol[g]	1
(*R*)-Carteolol	Hydroxylation	1	Unknown	Glu-216[e], Phe-483	4	3	8-Hydroxy carteolol	2
(*S*)-Carteolol	Hydroxylation	1	Unknown	Glu-216[e], Ser-217, Phe-120[f], Val-370, Phe-483[f], Leu-484	3.5	1	8-Hydroxy carteolol	2
Codeine	*O*-Demethylation	1	Achiral	Glu-216[e], Phe-120[f], Phe-483[f], Leu-384[e]	3.6	4	Morphine	3
Debrisoquine	Hydroxylation	3	Achiral	Glu-216[e], Phe120, Phe-483[f]	4.2(4C)	11(4C), NP(1C), NP(3C)	4S-Hydroxy debrisoquine	1
Dextromethorphan	*O*-Demethylation	1	Achiral	Glu-216[e], Phe-120[f], Phe-483,Val-308, Leu-384	2.9	2	Dextrorphan	1
(*R*)-Fluoxetine	*N*-Demethylation	1	R + S	Ala-305, Phe-120[f], Val-370, Phe-483[f], Leu-384, Leu-121, Leu-220	3.9	5	*N*-Desmethyl fluoxetine	1
(*S*)-Fluoxetine	*N*-Demethylation	1	R + S	Phe120[f], Leu-121, Leu-220	3.7	14	*N*-Desmethyl fluoxetine	1
(*R*)-MDMA[h]	Demethylenation	1	R + S	Glu-216[e], Phe-120[f], Phe483[f], Leu-484	3.0	1	3,4-OH MA	1
(*S*)-MDMA	Demethylenation	1	R + S	Glu-216[e], Phe-120[f], Phe483[f], Leu-484	3.2	1	3,4-OH MA	1
(*R*)2-Methoxyamphetamine	*O*-Demethylation, Hydroxylation	3	Unknown	Glu-216[e], Phe-120, Phe-483	2.7(O), 3.2(5C), 4.3(3C)	1(O), 9(5C), 3(3C)	*O*-Desmethyl-amphetamine + 5-hydroxy methoxyamphetamine	1
(*S*)2-Methoxyamphetamine	*O*-Demethylation, hydroxylation	3	Unknown	Glu-216[e], Phe-120, Phe-483	4.4(O), 3.5(5C), 4.0(3C)	1(O), 6(5C), 3(3C)	*O*-Desmethyl-amphetamine + 5-hydroxy methoxyamphetamine	1
(*R*)-Metoprolol	*O*-Demethylation	2	R + S	Glu-216[e], Asp-301[e], Phe-120[f], Phe-483	3.5(O), 3.9(αC)	2(O), 9(αC)	*O*-Desmethylmetoprolol	1
(*S*)-Metoprolol	Hydroxylation	2	R + S	Glu-216[e], Asp301	2.9(O), 4.0(αC)	11(O), 1(αC)	α-Hydroxymetoprolol	1
(*R*)-Mexiletine	Hydroxylation	2	R + S	Glu-216[e] Phe-120[f], Phe-483[f], Leu-484	3.0(Me), 3.2(4C)	1(Me), 2(4C)	4-Hydroxy mexiletine + 2-hydroxymethyl mexiletine	1
(*S*)-Mexiletine	Hydroxylation	2	R + S	Glu-216[e], Phe-120[f]	3.0(Me), 3.3(4C)	10(Me), 1(4C)	4-Hydroxy mexiletine + 2-hydroxymethyl mexiletine	1
(*R*)-Mianserin	Hydroxylation	2	R + S	Glu-216[e], Phe-120[f], Phe-483[f]	4.4(8C), 3.2(N)	1(8C), 2(N)	8-Hydroxymianserin	1
(*S*)-Mianserin	Hydroxylation	2	R + S	Glu-216[e], Phe-120[f]	4.0(8C)	6(8C)	8-Hydroxymianserin	2

Table 4 continued

Substrate	Major metabolic transformation	No of sites of metabolism	Chiral preference	Key residues in close contact with ligand[c]	Oxeme-SoM best pose distance[a]	Best ranked pose nearest to oxeme[b]	Major metabolite	No of atoms within 4.5 Å cutoff[d]
Progesterone	Hydroxylation	4	Chiral	Phe-120, Phe-483	3.8(6C), 3.8(21C)	1(6C), 12(21C), NP(2C), NP(16C)	2β + 6β + 16α + 21-Hydroxylprogesterone	2
Spirosulfonamide	Hydroxylation	1	Achiral	Phe-120, Gln-244[e]	3.3	1	7-Hydroxyspirosulfonamide[g]	1
Tolterodine	Hydroxylation	1	R	Glu-216[e], Phe-120, Phe-483, Val-370, Leu-484	2.6	5	5-Hydroxymethyl tolterodine	1
(*R*)-Venlafaxine	*O*-Demethylation	1	R + S	Glu-216, Phe-120[f], Phe-483[f], Leu-213, Leu-484	3.9	1	*O*-Desmethylvenlafaxine	1
(*S*)-Venlafaxine[h]	*O*-Demethylation	1	R + S	Glu-216[e], Phe-120, Phe-483, Leu-213, Leu-484	3.8	1	*O*-Desmethylvenlafaxine	1

[a] Distance in Å of the best docked pose from Oxeme to the SoM site. For multiple sites of metabolism, value in parenthesis denotes the SoM site. *O* and *N* refer to *O*-demethylation and *N*-dealkylation

[b] Best Ranked Pose where SoM site is nearest to Oxeme. NP designates 'No pose found'

[c] Critical residues (hydrophobic and hydrogen bond interactions) involved in substrate recognition which are at a distance of <4 Å from any atom of the substrate

[d] No. of atoms in the best pose which are within the 4.5 Å cutoff distance from the oxeme heme

[e] Hydrogen bond within 3.5 Å

[f] π–π interaction, i.e., centroid of aromatic rings stacked in an antiparallel fashion within 4 Å

[g] Sterochemistry of product unknown

[h] Stereoisomers that are disfavored, but still act as weak CYP2D6 substrates

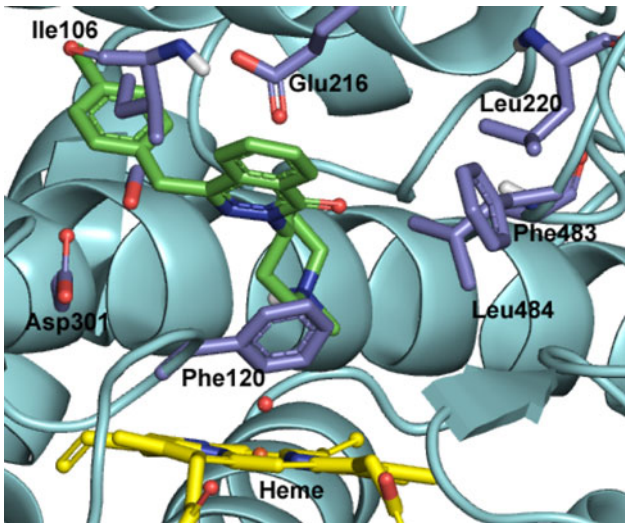

Fig. 7 Docked pose of (*R*)-azelastine in the CYP2D6 homology model

was within the distance cut-off of 4.5 Å denoting a docking success (Fig. 7). The oxeme to methyl carbon distance was 3.20 Å while the oxeme to basic nitrogen distance was 3.75 Å. The basic nitrogen of azelastine was pointed towards the heme and in position to form a favorable electrostatic interaction with the oxygen atom of the heme. There was tight packing of the azepane ring with Phe-120 and Leu-484 residues, while the oxophthalazine ring packed against Leu-121 and Ile-106 residues. There were no additional hydrogen bonds from the substrate to the protein. The chlorophenyl ring was placed near the Asp-301 side chain, but did not form any specific interactions with the protein. For (*S*)-azelastine, the 8th highest scoring pose had its SoM within the cut-off, with an oxeme to methyl carbon distance of 3.27 Å and oxeme to basic nitrogen distance of 4.23 Å. The overall fit of this pose in the CYP2D6 active site was similar to that observed for (*R*)-azelastine, with the basic nitrogen pointing towards the oxeme, but it was further away from the Ala-305 backbone carbonyl (4.18 Å). It is interesting to note that no docked poses were found for either azelastine isomer where the basic nitrogen interacts with either Glu-216 or Asp-301, which is an important element for orienting substrates toward the heme for the hydroxylation reaction. The steric constraints imposed by the protein active site do not appear to favor the oxophthalazine ring of azelastine to be positioned near the heme.

Bufuralol is a potent antihypertensive [52] that is oxidized to 1′-OH-bufuralol by CYP2D6. It shows clear substrate enantioselectivity for (*R*)-bufuralol [53] while still catalyzing oxidation of the disfavored stereoisomer to a more limited extent. Figure 8 illustrates the top scoring poses for both enantiomers of bufuralol. The top scoring pose for (*R*)-bufuralol placed the SoM 3.94 Å from the oxeme, well within the 4.5 Å cut-off. The internal distance from the basic nitrogen to the SoM was 8.45 Å. The basic nitrogen formed a salt bridge with the side chain of Glu-216 (2.78 Å) and the benzofuran ring packed tightly between Phe-120 and Phe-483, as illustrated in Fig. 8. The hydroxyl group on the substrate formed hydrogen bonds with the backbone carbonyl oxygen of Asp-301 (3.51 Å) and the side chain hydroxyl of Ser-304 (2.67 Å). While this hydroxyl group was positioned near the Asp-301 side chain, it could not interact directly with the carboxylic acid group due to the side chain's rotameric state. The top scoring pose for (*S*)-bufuralol placed the SoM just within the distance cut-off (4.46 Å), as illustrated in Fig. 8. The substrate was in an extended conformation within the binding pocket with an internal SoM to basic nitrogen distance of 8.52 Å, similar to that seen for the (*R*)-enantiomer. The basic nitrogen formed a salt bridge with the side chain of Glu-216 (2.60 Å). The benzofuran ring did not occupy the same space as (*R*)-bufuralol, and so did not pack tightly against Phe-120 and Phe-483. The hydroxyl group was able to form a hydrogen bond with the Ser-304 side chain (2.77 Å), but was positioned further away from the Asp-301 residue compared to the (*R*)-bufuralol docking pose.

Although there were several similarities between the docked (*R*)- and (*S*)-bufuralol poses, including salt bridges

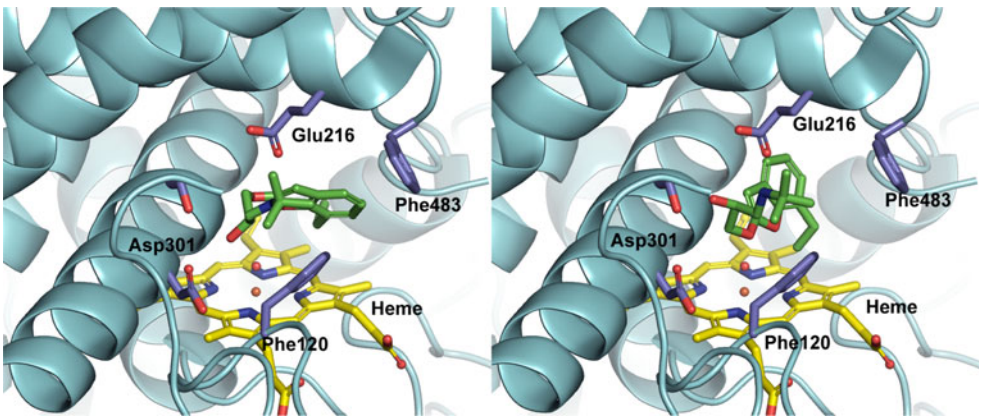

Fig. 8 Docked poses of (*R*)- and (*S*)-bufuralol (*left* and *right* figures, respectively) in the CYP2D6 homology model. Differences in the packing geometry of the benzofuran against the Phe-120 side chain may explain the observed CYP2D6 enantioselectivity

to Glu-216 and hydrogen bonds with Ser-304, it was striking that the benzofuran core occupied very different regions of the binding site depending on the stereoisomer. Mutation studies replacing Phe-120 with alanine (F120A) have shown that the substrate enantioselectivity observed in the wild-type does not exist with the mutant [53]. That we observed tight packing against Phe-120 with the (*R*)-enantiomer, but not with the (*S*) form, suggests that (*S*)-bufuralol may be unable to efficiently bind to the deeper part of the pocket due to the presence of the bulky phenyl side chain of Phe-120. Since our docking model indicates a role for the Ser-304 residue in bufaralol recognition, it will be interesting to see if S304A mutation [43] has a similar effect on the regio and enantioselective oxidation as seen in the case of debrisoquine and metoprolol ligands.

Dextromethorphan is a widely used antitussive that is metabolized via *O*- and *N*-demethylation, with the *O*-demethylation catalyzed by CYP2D6 [54]. There is evidence that CYP2D6 also catalyzes *N*-demethylation to a limited extent [55], however, metabolism at this site appears to occur only at very high concentrations that are not biologically relevant. The second docked pose of dextromethorphan placed the *O*-demethylation SoM within the cut-off (2.87 Å) and had the basic nitrogen in an (*S*)-configuration. The internal distance between the *O*-demethylation SoM and basic nitrogen was 7.29 Å. The basic nitrogen formed a salt bridge with Glu-216 at a distance of 2.61 Å and there was tight packing of the hydrophobic parts of the substrate with Phe-120, Val-308, Phe-483, and Leu-484.

Fluoxetine is a selective serotonin reuptake inhibitor (SSRI) antidepressant that is metabolized by CYP2D6 via *N*-demethylation with no apparent enantioselective preference [56]. The fifth highest scoring docked pose of (*R*)-fluoxetine placed the SoM within the cut-off, with an oxeme to carbon distance of 3.85 Å and an oxeme to nitrogen distance of 2.95 Å (Fig. 9). The basic nitrogen was oriented such that it formed a long range interaction with the backbone carbonyl of Ala-305 (3.62 Å). A closer inspection of this pose reveals the trifluoromethyl group lying adjacent to the Glu-216 residue in a position that one would expect to be electrostatically disfavored. Placement of the trifluoromethyl group in this position suggests that there may be reorganization of the protein in the region around the Glu-216 side chain on fluoxetine binding, but since our docking method provided no treatment for alternate side chain conformations this possibility was not captured in our calculations. It is quite possible that this disfavored electronic interaction between the CF3 group and Glu-216 residue results in the 3-phenyl group being further buried and packing against residues Phe-120, Val-370, Phe-483, and Leu-484. The first (*S*)-fluoxetine pose within the SoM to oxeme cut-off was the 14th in the ranked list of docked

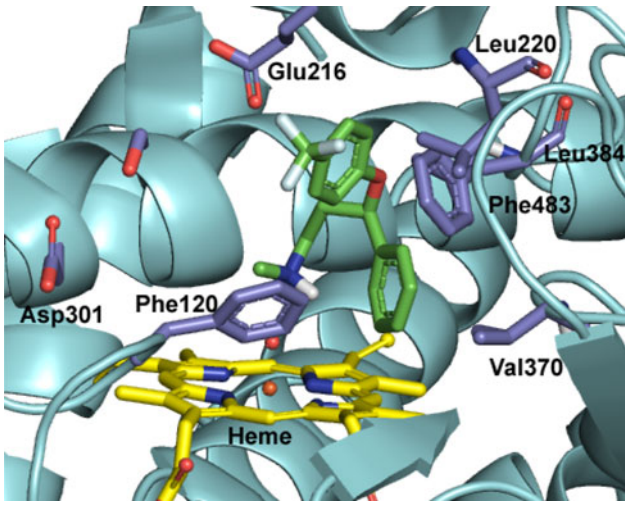

Fig. 9 (*R*)-Fluoxetine docked to the CYP2D6 homology model

poses (oxeme to carbon distance of 3.65 Å, oxeme to nitrogen distance of 2.86 Å). The basic nitrogen was distant from the Ala-305 carbonyl group, compared to the (*R*)-enantiomer, and the 3-phenyl group had shifted away from Val-370 and Phe-483 residues, but towards the hydrophobic pocket containing Phe-120. The trifluoromethyl phenyl group was in the same location as seen in (*R*)-fluoxetine. The higher scoring poses that did not correctly position the SoM all placed the basic nitrogen within a short distance of the Glu-216 side chain.

Based on these observations of the substrate poses, one can formulate a general hypothesis for substrate features that favor *N*-dealkylation over *O*-demethylation/hydroxylation (Fig. 10). For substrates such as azelastine or fluoxetine that favor CYP2D6 catalyzed *N*-dealkylation, the aromatic interaction with Phe-120 is the major stabilizing force, which is strengthened by additional hydrophobic interactions with Val-370, Leu-484, Phe-483 near the heme and Val-104, Ile-106, Leu-213, Leu-220 at the

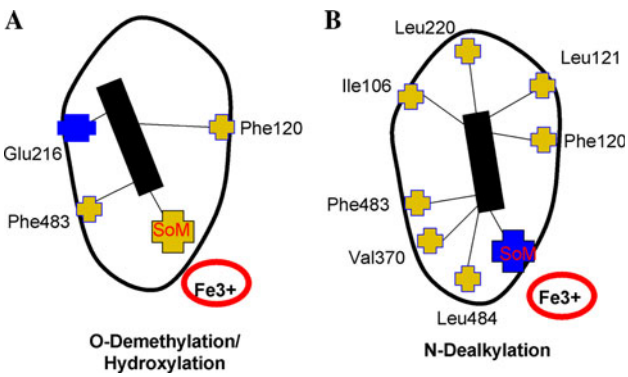

Fig. 10 A schematic diagram of the substrate binding modes which favor (**A**) *O*-demethylation and hydroxylation and (**B**) *N*-dealkylation. The basic nitrogen is colored in *blue* while hydrophobic interactions are shown in *yellow*

distal end. These hydrophobic interactions compensate for the absence of a strong electrostatic interaction between a basic nitrogen and Glu-216 residue. Additionally, steric constraints within the active site can also prevent substrates from orienting the basic nitrogen towards the Glu-216 residue, as seen in the case of azelastine. Substrates such as bufaralol and dextromethorphan, which allow hydroxylation and *O*-dealkylation, respectively, mainly rely on an interaction between their basic nitrogen and Glu-216 as the primary driver for binding, while an additional interaction exists between an aromatic region in the substrates and the Phe-120 and Phe-483 side chains. In view of the small number of cases studied here, it is not possible at this time to predict from docking studies which pathway would be preferred for a CYP2D6 substrate, however, a combined approach using pharmacophore, molecular orbital calculations and protein modeling has been shown to successfully predict metabolites from the pathways catalyzed by CYP2D6 [11].

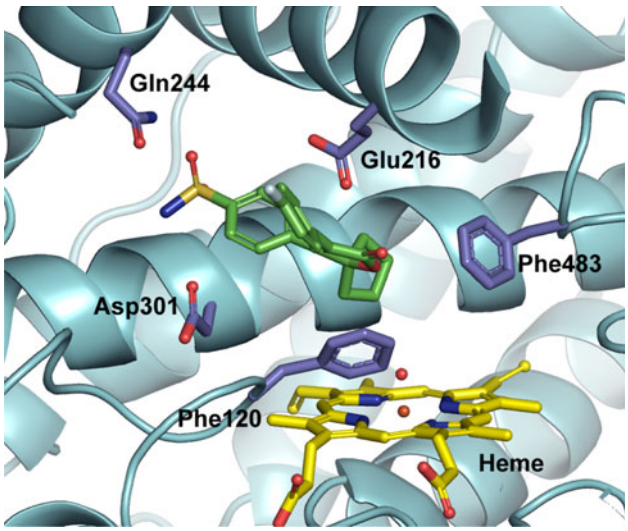

Fig. 11 Docked pose of spirosulfonamide in the CYP2D6 homology model. The sulfonamide group on the substrate hydrogen bonds to the Gln-244 side chain

Binding of substrates not containing a basic nitrogen

Although the classical pharmacophore for CYP2D6 substrates contains a basic nitrogen group, which presumably interacts with Glu-216, there are several known substrates that do not contain this feature. We included two of them in our study, progesterone and spirosulfonamide, and the CYP2D6 binding site finds unique ways to interact with each one.

Progesterone is a steroid hormone that is metabolized by CYP2D6 via 2β-, 6β-, 16α-, and 21-hydroxylation [12]. The top scoring docked pose for progesterone corresponded to 6β-hydroxylation, with a SoM to oxeme distance of 3.78 Å. The B, C, and D rings of progesterone stacked in parallel with the Phe-120 side chain, while the A ring was packed against Phe-483. The methyl ketone group was positioned in the space between Glu-216 and Asp-301, but made no apparent hydrogen bonds with the protein. The 12th pose positioned the 21-hydroxylation SoM 3.79 Å from the oxeme. Packing of the steroid scaffold against the active site phenylalanine side chains was not as tight as seen in the 6β-hydroxylation case described above, with only the C ring parallel to Phe-120 side chain and the D ring perpendicular to Phe-483. The carbonyl group on the A ring was positioned near the Asp-301 acidic side chain, but did not form any hydrogen bonding interactions to the protein. The 2β- and 16α-hydroxylation sites were not identified via docking.

Spirosulfonamide hydroxylation by CYP2D6 occurs at the "outer" methylene of the cyclopentyl ring [13]. The highest scoring docked pose had a distance from oxeme to SoM of 3.34 Å, as shown in Fig. 11, with the cyclopentyl ring packed against the Phe-120 side chain. The internal SoM to sulfonamide nitrogen distance was 9.20 Å. The sulfonamide moiety served as an anchor for correct positioning of the SoM towards the reactive oxeme of the heme, similar to the function of the basic nitrogen of other substrates; however, it accomplished this through different interactions with the protein. The amide nitrogen was positioned between the Asp-301 side chain (3.22 Å) and the carbonyl oxygen of the Gln-244 side chain (3.62 Å). One of the sulfonyl oxygen atoms of spirosulfonamide also formed a hydrogen bond with the amide nitrogen of the Gln-244 side chain. This set of interactions was unique compared to the other substrates in this study and spirosulfonamide was the only substrate to form hydrogen bonding interactions with the side chain of Gln-244. It is interesting to note that spirosulfonamide analogs where the sulfonamide moiety was modified to a methyl sulfone led to a $\sim$30 fold loss in CYP2D6 binding affinity [13], suggesting that Gln244 may play an important role in substrate recognition.

In the case of progesterone, there is little opportunity on the steroid scaffold to form hydrogen bonds with key residues of the CYP2D6 binding site. Instead, hydrophobic and ring stacking interactions against the phenylalanine residues appear to play the major role in binding. This is also consistent with the pattern of metabolic sites on progesterone, with several SoMs distributed on opposite sides of the scaffold. With no critical hydrogen bonds between substrate and protein required for binding, progesterone can adopt many configurations within the binding site and expose many parts of its scaffold to the catalytic center. On the other hand, spirosulfonamide replaces the salt bridge between substrate and protein with interactions to the Gln-

244 side chain, which acts as an anchor for positioning the substrate in the binding pocket much the same way that Glu-216 and Asp-301 help orient substrates.

Substrate size and number of metabolic sites

Examination of the primary literature for the CYP2D6 substrates led to an observation that the smaller substrates appeared more likely than the larger ones to have multiple sites of metabolism. An inspection of Fig. 6 shows that several of the smallest substrates (debrisoquine, methoxyamphetamine, metoprolol, mianserin, and mexiletine) all have multiple SoMs. The substrates that do not follow this trend are MDMA (MW = 194.3), with a single SoM, and progesterone (MW = 314.5) with four (see Tables 4, 5).

Figure 12 illustrates the relationship between the number of metabolic sites and both the molecular weight and clogP of the substrates. Correlation between the molecular weight and the number of metabolic sites was moderate, as measured by the Spearman rank-order correlation coefficient ($r_s = -0.52$), but statistically significant (two tailed p-value = 0.038). In contrast, there was no strong relationship between clogP and the number of metabolic sites. The Spearman rank-order correlation coefficient indicated low correlation between these values ($r_s = -0.33$) that was not able to differentiate substrate SoM count based on clogP (two tailed p-value = 0.21).

The substrate poses generated by molecular docking provided some insight for reasons that a relationship between substrate size and number of metabolic sites may exist. Several of the smallest substrates (i.e., debrisoquine, methoxyamphetamine, and mexiletine) appear to only occupy the region of the binding site between the catalytic center of the heme and the Glu-216 side chain. The salt bridge formed between the basic nitrogen of the substrates and Glu-216 provides an anchor point, allowing the rest of the substrate conformational freedom and the ability to position multiple moieties near the heme. This is essentially an argument that access to the heme is driving this relationship rather than the local reactivity of different regions of the substrates. Even in the case of slightly larger substrates like metoprolol, which extends further out into the binding pocket, both of its SoMs are close to each other on the same flexible tailpiece, indicating that the ability to adopt multiple conformations in this region of the binding site is of key importance. Many of the larger substrates are also more rigid, at least in the proximity of their SoMs, meaning that presentation of multiple sites to the catalytic center may be energetically unfavorable. In the case of progesterone, with four SoMs and a rigid steroid scaffold, flexibility in binding conformation is achieved by having no specific anchoring interaction with the protein, as described in the preceding section, giving it the opportunity to completely flip its orientation in the binding site.

Table 5 Molecular weight and cLogP Properties of the CYP2D6 substrates

Compound	Molecular weight	cLogP
Azelastine	382.9	4.4
Bufuralol	292.4	4.1
Carteolol	293.4	1.8
Codeine	300.4	1.6
Debrisoquine	176.2	1.2
Dextromethorphan	272.4	4.5
Fluoxetine	310.3	5.1
MDMA	194.3	2.5
2-Methoxyamphetamine	166.2	1.7
Metoprolol	268.4	2.0
Mexiletine	180.3	2.6
Mianserin	265.4	4.6
Progesterone	314.5	3.8
Spirosulfonamide	387.4	3.2
Tolterodine	326.5	5.7
Venlafaxine	278.4	3.6

At first, these results appear contradictory to the notion that increasing the size of a compound (i.e., molecular weight) increases the potential for toxicity and metabolic liability. However, this rule of thumb accounts for the sum total of metabolic processes catalyzed by different CYPs that chemical compounds undergo physiologically, while our results address only the reactions catalyzed by CYP2D6, meaning that these trends should not necessarily correlate. In addition, our dataset is small and an analysis including many more known CYP2D6 substrates would be necessary to provide further verification of our observation. It is possible that including a substrate reactivity component, such as one based on a combined molecular orbital calculation and fragment recognition approach within MetaSite, may make the multiple metabolic site predictions better.

Conclusions

The aim of the current study was to see if a docking strategy that is fast, easy to use and computationally inexpensive can be used to predict CYP2D6 substrate metabolism. The paper describes the building, refinement, and validation of a homology model of CYP2D6 based on substrate-bound X-ray structures of CYP2C5. The homology model was used in docking studies within Glide to predict the site of metabolism for a range of known CYP2D6 substrates and identify key residues in the active site that are responsible for ligand recognition.

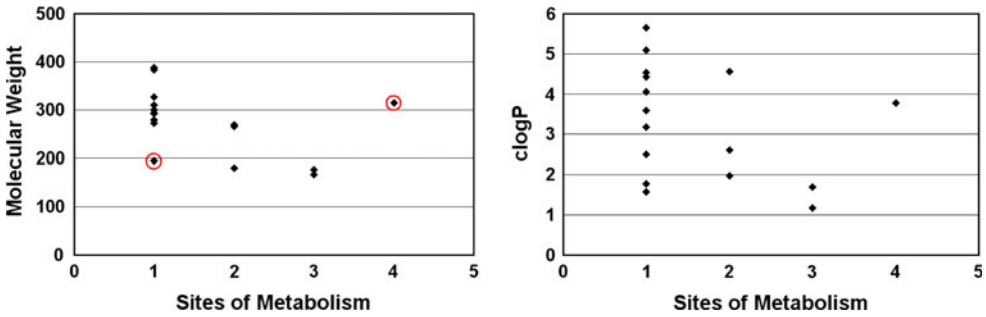

Fig. 12 Plots showing the relationship between MW, clogP and the number of metabolic sites on the substrates. Outliers that do not follow the MW vs. SoM trend (MDMA with one SoM and progesterone with four SoMs) are indicated by *red circles*

Examination of the top 5 scoring poses showed that for 85% of the substrates, the predicted metabolic sites are consistent with known oxidation patterns of these substrates. Furthermore these results show that the best pose observed in 80% of the substrates had only a single atom, i.e., the correct SoM, within the 4.5 Å cutoff. (see Table 4). Although the homology model was found to be in good agreement with the recently solved apo crystal structure of CYP2D6, there were structural differences between them. These differences highlight the issue of substrate induced changes in the active site, as seen by the loss in accuracy in predicting the correct site of metabolism when the apo form X-ray structure was used for docking. Clearly, one of the key challenges that remain in CYP docking is the treatment of target flexibility that can account for induced-fit adaptations of protein upon ligand binding. Indeed, much effort over the past several years has been in developing new docking algorithms that allow side chain flexibility and scoring of flexible ligands in the active site. Other approaches that are more computationally expensive such as ensemble docking, that involves docking ligands to a small number of protein conformations, have been shown to give better enrichment [57] than using just a single structure. Induced fit docking methods [58] where protein is "induced" into the correct binding conformation for a given ligand also lead to better docking results when compared to rigid receptor docking and recently a combined molecular dynamics and decision tree [59] approach were found to be successful in improving the reliability of SoM predictions (80%) of known CYP2D6 substrates. Lastly, more work is needed to study the effect of the various CYP2D6 polymorphs on substrate metabolism.

Supporting information available

Ramachandran plot for the CYP2D6 homology model and detailed docking descriptions for substrates not fully discussed in the main text. This material is available free of charge via the Internet at http://pubs.acs.org. Figures were constructed using the Pymol program (http://www.pymol.org/).

Acknowledgments The authors thank Yuchen Bai from the Wyeth Bioinformatics Department for his help with sequence analysis of CYP2D6 polymorphs and Will Somers for support of this work.

References

1. Kola I, Landis J (2004) Opinion: can the pharmaceutical industry reduce attrition rates? Nat Rev Drug Discov 3:711–716
2. Danielson PB (2002) The cytochrome P 450 superfamily: biochemistry, evolution and drug metabolism in humans. Curr Drug Metab 3:561–597
3. Auclair K, Hu Z, Little DM, Ortiz de Montellano PR, Groves JT (2002) Revisiting the mechanism of P450 enzymes with the radical clocks norcarane and spiro[2,5]octane. J Am Chem Soc 124:6020–6027
4. Bertz RJ, Granneman GR (1997) Use of in vitro and in vivo data to estimate the likelihood of metabolic pharmacokinetic interactions. Clin Pharmacokinet 32:210–258
5. Bertilsson L, Dahl M-L, Dalen P, Al-Shurbaji A (2002) Molecular genetics of CYP2D6: clinical relevance with focus on psychotropic drugs. Br J Clin Pharmacol 53:111–122
6. Strobl GR, von Kruedener S, Stoeckigt J, Guengerich FP, Wolff T (1993) Development of a pharmacophore for inhibition of human liver cytochrome P-450 2D6: molecular modeling and inhibition studies. J Med Chem 36:1136–1145
7. Michalets EL (1998) Update: clinically significant cytochrome P-450 drug interactions. Pharmacotherapy 18:84–112
8. Lennard MS (1990) Genetic polymorphism of sparteine/debrisoquine oxidation: a reappraisal. Pharmacol Toxicol 67:273–283
9. Cruciani G, Carosati E, De Boeck B, Ethirajulu K, Mackie C, Howe T, Vianello R (2005) MetaSite: understanding metabolism in human cytochromes from the perspective of the chemist. J Med Chem 48:6970–6979
10. Trunzer M, Faller B, Zimmerlin A (2009) Metabolic soft spot identification and compound optimization in early discovery phases using MetaSite and LC-MS/MS validation. J Med Chem 52:329–335
11. De Groot MJ, Ackland MJ, Horne VA, Alex AA, Jones BC (1999) A novel approach to predicting P450 mediated drug metabolism. CYP2D6 catalyzed *N*-dealkylation reactions and qualitative metabolite predictions using a combined protein and pharmacophore model for CYP2D6. J Med Chem 42:4062–4070
12. Hiroi T, Kishimoto W, Chow T, Imaoka S, Igarashi T, Funae Y (2001) Progesterone oxidation by cytochrome P450 2D isoforms in the brain. Endocrinology 142:3901–3908
13. Guengerich FP, Miller GP, Hanna IH, Martin MV, Leger S, Black C, Chauret N, Silva JM, Trimble LA, Yergey JA, Nicoll-Griffith DA (2002) Diversity in the oxidation of substrates by cytochrome P450 2D6: lack of an obligatory role of aspartate 301-substrate electrostatic bonding. Biochemistry 41:11025–11034

14. Yano JK, Hsu M-H, Griffin KJ, Stout CD, Johnson EF (2005) Structures of human microsomal cytochrome P450 2A6 complexed with coumarin and methoxsalen. Nat Struct Mol Biol 12:822–823
15. Yano JK, Wester MR, Schoch GA, Griffin KJ, Stout CD, Johnson EF (2004) The structure of human microsomal cytochrome P450 3A4 determined by X-ray crystallography to 2.05-Å resolution. J Biol Chem 279:38091–38094
16. Williams PA, Cosme J, Vinkovic DM, Ward A, Angove HC, Day PJ, Vonrhein C, Tickle IJ, Jhoti H (2004) Crystal structures of human cytochrome P450 3A4 bound to metyrapone and progesterone. Science 305:683–686
17. Wester MR, Johnson EF, Marques-Soares C, Dijols S, Dansette PM, Mansuy D, Stout CD (2003) Structure of mammalian cytochrome P450 2C5 complexed with diclofenac at 2.1 Å resolution: evidence for an induced fit model of substrate binding. Biochemistry 42:9335–9345
18. Wester MR, Johnson EF, Marques-Soares C, Dansette PM, Mansuy D, Stout CD (2003) Structure of a substrate complex of mammalian cytochrome P450 2C5 at 2.3 Å resolution: evidence for multiple substrate binding modes. Biochemistry 42:6370–6379
19. Williams PA, Cosme J, Ward A, Angove HC, Vinkovic DM, Jhoti H (2003) Crystal structure of human cytochrome P450 2C9 with bound warfarin. Nature 424:464–468
20. Wester MR, Yano JK, Schoch GA, Yang C, Griffin KJ, Stout CD, Johnson EF (2004) The structure of human cytochrome P 450 2C9 complexed with flurbiprofen at 2.0-Å resolution. J Biol Chem 279:35630–35637
21. Scott EE, He YA, Wester MR, White MA, Chin CC, Halpert JR, Johnson EF, Stout CD (2003) An open conformation of mammalian cytochrome P 450 2B4 at 1.6-Å resolution. Proc Natl Acad Sci USA 100:13196–13201
22. Rowland P, Blaney Frank E, Smyth Martin G, Jones Jo J, Leydon Vaughan R, Oxbrow Amanda K, Lewis Ceri J, Tennant Mike G, Modi S, Eggleston Drake S, Chenery Richard J, Bridges Angela M (2006) Crystal structure of human cytochrome P450 2D6. J Biol Chem 281:7614–7622
23. de Graaf C, Oostenbrink C, Keizers PHJ, van der Wijst T, Jongejan A, Vermeulen NPE (2006) Catalytic site prediction and virtual screening of cytochrome P450 2D6 substrates by consideration of water and rescoring in automated docking. J Med Chem 49:2417–2430
24. Schrodinger, Glide version 4.5, LLC, Portland, OR, USA, 2007
25. de Graaf C, Vermeulen NPE, Feenstra KA (2005) Cytochrome P450 in silico: an integrative modeling approach. J Med Chem 48:2725–2755
26. Lewis David FV, Dickins M, Lake Brian G, Goldfarb Peter S (2003) A molecular model of CYP2D6 constructed by homology with the CYP2C5 crystallographic template: investigation of enzyme–substrate interactions. Drug Metabol Drug Interact 19:189–210
27. Venhorst J, ter Laak AM, Commandeur JNM, Funae Y, Hiroi T, Vermeulen NPE (2003) Homology modeling of rat and human cytochrome P450 2D (CYP2D) isoforms and computational rationalization of experimental ligand-binding specificities. J Med Chem 46:74–86
28. de Graaf C, Oostenbrink C, Keizers PHJ, van Vugt-Lussenburg BMA, van Waterschoot RAB, Tschirret-Guth RA, Commandeur JNM, Vermeulen NPE (2007) Molecular modeling-guided site-directed mutagenesis of cytochrome P450 2D6. Curr Drug Metab 8:59–77
29. Sali A, Blundell TL (1993) Comparative protein modeling by satisfaction of spatial restraints. J Mol Biol 234:779–815
30. Shen M-Y, Sali A (2006) Statistical potential for assessment and prediction of protein structures. Protein Sci 15:2507–2524
31. Davis IW, Murray LW, Richardson JS, Richardson DC (2004) MolPROBITY: structure validation and all-atom contact analysis for nucleic acids and their complexes. Nucleic Acids Res 32:W615–W619
32. Modi S, Paine MJ, Sutcliffe MJ, Lian LY, Primrose WU, Wolf CR, Roberts GC (1996) A model for human cytochrome P450 2D6 based on homology modeling and NMR studies of substrate binding. Biochemistry 35:4540–4550
33. Schrodinger, Maestro version 7.5.116, LLC, Portland, OR, USA, 2006
34. Jorgensen WL, Maxwell DS, Tirado-Rives J (1996) Development and testing of the OPLS all-atom force field on conformational energetics and properties of organic liquids. J Am Chem Soc 118:11225–11236
35. Halgren TA (1996) Merck molecular force field. V. Extension of MMFF94 using experimental data, additional computational data, and empirical rules. J Comput Chem 17:616–641
36. Friesner RA, Banks JL, Murphy RB, Halgren TA, Klicic JJ, Mainz DT, Repasky MP, Knoll EH, Shelley M, Perry JK, Shaw DE, Francis P, Shenkin PS (2004) Glide: a new approach for rapid, accurate docking and scoring. 1. Method and assessment of docking accuracy. J Med Chem 47:1739–1749
37. Halgren TA, Murphy RB, Friesner RA, Beard HS, Frye LL, Pollard WT, Banks JL (2004) Glide: a new approach for rapid, accurate docking and scoring. 2. Enrichment factors in database screening. J Med Chem 47:1750–1759
38. Friesner RA, Murphy RB, Repasky MP, Frye LL, Greenwood JR, Halgren TA, Sanschagrin PC, Mainz DT (2006) Extra precision glide: docking and scoring incorporating a model of hydrophobic enclosure for protein–ligand complexes. J Med Chem 49:6177–6196
39. Flanagan JU, Marechal J-D, Ward R, Kemp CA, McLaughlin LA, Sutcliffe MJ, Roberts GCK, Paine MJI, Wolf CR (2004) Phe120 contributes to the regiospecificity of cytochrome P450 2D6: mutation leads to the formation of a novel dextromethorphan metabolite. Biochem J 380:353–360
40. Paine MJI, McLaughlin LA, Flanagan JU, Kemp CA, Sutcliffe MJ, Roberts GCK, Wolf CR (2003) Residues glutamate 216 and aspartate 301 are key determinants of substrate specificity and product regioselectivity in cytochrome P450 2D6. J Biol Chem 278:4021–4027
41. Gotoh O (1992) Substrate recognition sites in cytochrome P450 family 2 (CYP2) proteins inferred from comparative analyses of amino acid and coding nucleotide sequences. J Biol Chem 267:83–90
42. McLaughlin LA, Paine MJI, Kemp CA, Marechal J-D, Flanagan JU, Ward CJ, Sutcliffe MJ, Roberts GCK, Wolf CR (2005) Why is quinidine an inhibitor of cytochrome P450 2D6?: the role of key active-site residues in quinidine binding. J Biol Chem 280:38617–38624
43. Ellis SW, Hayhurst GP, Lightfoot T, Smith G, Harlow J, Rowland-Yeo K, Larsson C, Mahling J, Lim CK, Wolf CR, Blackburn MG, Lennard MS, Tucker GT (2000) Evidence that serine 304 is not a key ligand-binding residue in the active site of cytochrome P450 2D6. Biochem J 345:565–571
44. Ellis SW, Rowland K, Ackland MJ, Rekka E, Simula AP, Lennard MS, Wolf CR, Tucker GT (1996) Influence of amino acid residue 374 of cytochrome P-450 2D6 (CYP2D6) on the regio- and enantio-selective metabolism of metoprolol. Biochem J 316:647–654
45. Hayhurst GP, Harlow J, Chowdry J, Gross E, Hilton E, Lennard MS, Tucker GT, Ellis SW (2001) Influence of phenylalanine-481 substitutions on the catalytic activity of cytochrome P450 2D6. Biochem J 355:373–379
46. Ellis SW, Hayhurst GP, Smith G, Lightfoot T, Wong MMS, Simula AP, Ackland MJ, Sternberg MJE, Lennard MS et al

(1995) Evidence that aspartic acid 301 is a critical substrate-contact residue in the active site of cytochrome P450 2D6. J Biol Chem 270:29055–29058
47. Kirton SB, Kemp CA, Tomkinson NP, St.-Gallay S, Sutcliffe MJ (2002) Impact of incorporating the 2C5 crystal structure into comparative models of cytochrome P450 2D6. Proteins Struct Funct Genet 49:216–231
48. Guengerich FP, Hanna IH, Martin MV, Gillam EMJ (2003) Role of glutamic acid 216 in cytochrome P450 2D6 substrate binding and catalysis. Biochemistry 42:1245–1253
49. Keizers PHJ, Lussenburg BMA, de Graaf C, Mentink LM, Vermeulen NPE, Commandeur JNM (2004) Influence of phenylalanine 120 on cytochrome P450 2D6 catalytic selectivity and regiospecificity: crucial role in 7-methoxy-4-(aminomethyl)-coumarin metabolism. Biochem Pharmacol 68:2263–2271
50. Imai T, Taketani M, Suzu T, Kusube K, Otagiri M (1999) In vitro identification of the human cytochrome P-450 enzymes involved in the *N*-demethylation of azelastine. Drug Metab Dispos 27:942–946
51. Nakajima M, Nakamura S, Tokudome S, Shimada N, Yamazaki H, Yokoi T (1999) Azelastine *N*-demethylation by cytochrome P-450 (CYP)3A4, CYP2D6, and CYP1A2 in human liver microsomes: evaluation of approach to predict the contribution of multiple CYPs. Drug Metab Dispos 27:1381–1391
52. Johnston GD, Finch MB, Shanks RG (1986) Peripheral vascular effects of bufuralol in hypertensive and normal subjects: a comparison with propranolol and pindolol. Eur J Clin Pharmacol 30:649–652
53. Masuda K, Tamagake K, Okuda Y, Torigoe F, Tsuzuki D, Isobe T, Hichiya H, Hanioka N, Yamamoto S, Narimatsu S (2005) Change in enantioselectivity in bufuralol 1″-hydroxylation by the substitution of phenylalanine-120 by alanine in cytochrome P450 2D6. Chirality 17:37–43
54. Kerry NL, Somogyi AA, Bochner F, Mikus G (1994) The role of CYP2D6 in primary and secondary oxidative metabolism of dextromethorphan: in vitro studies using human liver microsomes. Br J Clin Pharmacol 38:243–248
55. Yu A, Dong H, Lang D, Haining RL (2001) Characterization of dextromethorphan *O*- and *N*-demethylation catalyzed by highly purified recombinant human CYP2D6. Drug Metab Dispos 29: 1362–1365
56. Margolis JM, O'Donnell JP, Mankowski DC, Ekins S, Obach RS (2000) (*R*)-, (*S*)-, and racemic fluoxetine *N*-demethylation by human cytochrome P450 enzymes. Drug Metab Dispos 28:1187–1191
57. Rao S, Sanschagrin PC, Greenwood JR, Repasky MP, Sherman W, Farid R (2008) Improving database enrichment through ensemble docking. J Comput Aided Mol Des 22:621–627
58. Sherman W, Day T, Jacobson MP, Friesner RA, Farid R (2006) Novel procedure for modeling ligand/receptor induced fit effects. J Med Chem 49:534–553
59. Hritz J, de Ruiter A, Oostenbrink C (2008) Impact of plasticity and flexibility on docking results for cytochrome P450 2D6: a combined approach of molecular dynamics and ligand docking. J Med Chem 51:7469–7477
60. Kudo S, Uchida M, Odomi M (1997) Metabolism of carteolol by cDNA-expressed human cytochrome P450. Eur J Clin Pharmacol 52:479–485
61. Dayer P, Desmeules J, Leemann T, Striberni R (1988) Bioactivation of the narcotic drug codeine in human liver is mediated by the polymorphic monooxygenase catalyzing debrisoquine 4-hydroxylation (cytochrome P-450 dbl/bufI). Biochem Biophys Res Commun 152:411–416
62. Eiermann B, Edlund PO, Tjernberg A, Dalen P, Dahl M-L, Bertilsson L (1998) 1- and 3-Hydroxylations, in addition to 4-hydroxylation, of debrisoquine are catalyzed by cytochrome P450 2D6 in humans. Drug Metab Dispos 26:1096–1101
63. Lightfoot T, Ellis SW, Mahling J, Ackland MJ, Blaney FE, Bijloo GJ, De Groot MJ, Vermeulen NPE, Blackburn GM, Lennard MS, Tucker GT (2000) Regioselective hydroxylation of debrisoquine by cytochrome P4502D6: implications for active site modelling. Xenobiotica 30:219–233
64. Kalant H (2001) The pharmacology and toxicology of "ecstasy" (MDMA) and related drugs. Can Med Assoc J 165:917–928
65. Meyer MR, Peters FT, Maurer HH (2008) The role of human hepatic cytochrome P450 isozymes in the metabolism of racemic 3,4-methylenedioxymethamphetamine and its enantiomers. Drug Metab Dispos 36:2345–2354
66. Geertsen S, Foster BC, Wilson DL, Cyr TD, Casley W (1995) Metabolism of methoxyphenamine and 2-methoxyamphetamine in P4502D6-transfected cells and cell preparations. Xenobiotica 25:895–906
67. Bach MV, Coutts RT, Baker GB (1999) Involvement of CYP2D6 in the in vitro metabolism of amphetamine, two *N*-alkylamphetamines and their 4-methoxylated derivatives. Xenobiotica 29:719–732
68. Abraham WT (2000) Beta-blockers: the new standard of therapy for mild heart failure. Arch Intern Med 160:1237–1247
69. Singh BN, Williams EMV (1972) Mode of action of a new antidysrhythmic drug, Ko 1173. Br J Pharmacol 44:1–9
70. Dejgard A, Petersen P, Kastrup J (1988) Mexiletine for treatment of chronic painful diabetic neuropathy. Lancet 1:9–11
71. Knoche B, Gehrcke B, Koenig A, Wainer IW (1996) Determination of the enantiomeric composition of mexiletine and its four hydroxylated metabolites in urine by enantioselective capillary gas chromatography. Chirality 8:30–34
72. Chow T, Hiroi T, Imaoka S, Chiba K, Funae Y (1999) Isoform-selective metabolism of mianserin by cytochrome P-450 2D. Drug Metab Dispos 27:1200–1204
73. Postlind H, Danielson A, Lindgren A, Andersson SHG (1998) Tolterodine, a new muscarinic receptor antagonist, is metabolized by cytochromes P450 2D6 and 3A in human liver microsomes. Drug Metab Dispos 26:289–293
74. Brynne N, Svanstrom C, Aberg-Wistedt A, Hallen B, Bertilsson L (1999) Fluoxetine inhibits the metabolism of tolterodine-pharmacokinetic implications and proposed clinical relevance. Br J Clin Pharmacol 48:553–563
75. Eap CB, Lessard E, Baumann P, Brawand-Amey M, Yessine M-A, O'Hara G, Turgeon J (2003) Role of CYP2D6 in the stereoselective disposition of venlafaxine in humans. Pharmacogenetics 13:39–47